

WAVE-DRIVEN TURBULENT CORONAL HEATING IN OPEN FIELD LINE REGIONS: NONLINEAR PHENOMENOLOGICAL MODEL

P. DMITRUK, L. J. MILANO, AND W. H. MATTHAEUS

Bartol Research Institute, University of Delaware, Newark, DE 19716; pablo@bartol.udel.edu

Received 2000 July 31; accepted 2000 September 26

ABSTRACT

A model is presented to investigate the driving of coronal turbulence in open field line regions, powered by low-frequency oscillatory field line motions at the coronal base. The model incorporates the combined effects of wave propagation, reflection associated with gradients of Alfvén speed, and low-frequency quasi-two-dimensional turbulence, which is treated using a one-point closure phenomenology appropriate to a transverse cascade in the reduced magnetohydrodynamic regime. Considering a sample of the corona and employing open boundary conditions, we use the model to investigate the dynamical efficiency of turbulent dissipation, which competes with propagation of fluctuations away from the coronal base. We examine the dependence of the heating efficiency on wave-forcing frequency, the sensitivity to parameters controlling the Alfvén speed profile, the behavior of the model for varying the phenomenological correlation length of turbulence, including asymptotic limits of negligible or very intense nonlinearities, and the confinement of turbulent dissipation to the region near the coronal base. Each of these issues may be of importance in understanding the heating of the corona and the origin of the solar wind.

Subject headings: MHD — Sun: corona — turbulence

1. INTRODUCTION

A promising model of coronal heating in open magnetic field line regions, based on MHD turbulence driven by reflections of low-frequency Alfvén waves, has been presented in Matthaeus et al. (1999a). To demonstrate the essential physics of this model, a simplified approach was taken, averaging fluctuations propagation and reflection over an MHD coronal box and considering a phenomenological nonlinear term to account for turbulent energy dissipation. Exact treatment of the nonlinear terms, through direct numerical simulations, is considered in Oughton et al. (2001), although propagation and reflection of waves is still averaged in the propagation direction. We proceed here in another intermediate step toward a complete model by considering a more detailed description of propagation and reflection but keeping the phenomenological approach for the nonlinear terms. This allows us to relate the model with previous studies of linear Alfvén waves propagating in a nonuniform media.

Various studies of coronal heating stand as antecedents to the present paper, although we emphasize that we as yet are not attempting embed our basic mechanism into a realistic coronal or wind model. Fluid plasma models for heating the coronal and accelerating the wind have been available for some time (e.g., Holzer & Axford 1970). These are often typified by use of an ad hoc “heating function” (McKenzie, Banaszekiewicz, & Axford 1995; Habbal et al. 1995; Evje & Leer 1998), which serves to demonstrate the necessity for the addition of requisite levels of plasma thermal energy through some unspecified process. Parker (1991) has argued that waves cannot be dissipated rapidly enough in the corona to account for adequate heat deposition and suggests instead that quasi-static motions must be responsible for driving coronal MHD activity. In contrast, Axford & McKenzie (1997) argue instead for an upward flux of Alfvén waves of sufficiently high frequency that they readily damp through kinetic processes that act at cyclotron scales. A number of studies (Tu & Marsch 1997;

Cranmer, Field, & Cole 1999) have examined both the effectiveness and the signatures of the cyclotron wave-damping mechanism. The suggestion that turbulence is involved in coronal heating dates at least to the studies of Coleman (1968) and van Ballegoijen (1986), who envisioned cascade processes in the corona that drive excitations from large scales down to smaller dissipative scales. Turbulent coronal heating, including reduced magnetohydrodynamics (RMHD) or MHD two-dimensional models and numerical simulations, has been widely discussed in connection with closed field line regions, especially loops (Gómez & Ferro-Fontán 1992; Heyvaerts & Priest 1992; Hendrix & van Hoven 1996; Einaudi et al. 1996; Dmitruk, Gómez, & DeLuca 1998) but only recently is being considered in open field line regions of the lower corona (Matthaeus et al. 1999a; Oughton et al. 2001), where a critical difference is that the fluctuations can escape from the region in which heating is required through wave propagation.

Generally cascade models have not described the associated dissipative mechanisms in any detail, although it has recently been argued (Leamon et al. 2000) that the compatibility of available dissipation processes with a highly anisotropic cascade (e.g., Matthaeus et al. 1998) would represent a significant constraint on heating models. Here we continue our earlier study in which dissipation occurs through a cascade that is driven by waves supplied at the coronal base. The cascade is highly anisotropic and is therefore described by RMHD equations that will be given below. The key issues examined below are related to the driving of a strong cascade by reflection, which itself is controlled by a coronal field and density model. We present a relatively tractable phenomenological model for examining this issue, thus complementing our earlier ongoing efforts to treat a wave-driven coronal cascade through direct numerical simulation.

2. MHD MODEL AND EQUATIONS

We consider a model based on the theory of transport of

small-scale MHD turbulence developed by Zhou & Matthaeus (1990) (see also Tu & Marsch 1989; Marsch & Tu 1993). The approach focuses on the dynamics of the small-scale fluctuations as influenced by specified large-scale inhomogeneities as well as by local nonlinear couplings.

The velocity and magnetic fields are decomposed into fluctuations and spatially slowly varying means,

$$\mathbf{V} = \mathbf{U} + \mathbf{v} \quad (1)$$

$$\mathbf{B} = \mathbf{B}_0 + \mathbf{b}. \quad (2)$$

The fluctuating components are then combined into the Elsässer fields,

$$\mathbf{z}_{\pm} = \mathbf{v} \pm \frac{1}{\sqrt{4\pi\rho}} \mathbf{b}. \quad (3)$$

Alfvén velocity $V_A = B_0/\sqrt{4\pi\rho}$ is defined in terms of the large-scale magnetic field and the background density field ρ , and it is also a slowly varying quantity.

The MHD equations for the small-scale fluctuations (Zhou & Matthaeus 1990) are

$$\begin{aligned} \frac{\partial \mathbf{z}_{\pm}}{\partial t} + (\mathbf{U} \mp V_A) \cdot \nabla \mathbf{z}_{\pm} + \frac{(\mathbf{z}_{\pm} - \mathbf{z}_{\mp})}{2} \cdot \nabla \cdot \left(\frac{\mathbf{U}}{2} \pm V_A \right) \\ + \mathbf{z}_{\mp} \cdot (\nabla \mathbf{U} \pm \frac{1}{\sqrt{4\pi\rho}} \nabla \mathbf{B}_0) \\ = -\frac{1}{\rho} \nabla p + N_{L\pm} + \mathbf{D}_{\pm}, \end{aligned} \quad (4)$$

where $N_{L\pm}$ represents nonlinear terms involving small-scale fluctuations couplings and \mathbf{D}_{\pm} are the dissipation terms.

We will consider an open field line region of the low corona between one and two solar radii, in which case we will work in the limit $U \ll V_A$, i.e., no wind flow is advecting the fluctuations. Moreover, we will assume the reduced MHD approximation (Strauss 1976; Montgomery 1982; Zank & Matthaeus 1992) in which fluctuations are perpendicular to the mean magnetic field and dependent on all spatial coordinates, but with a slow variation along the mean magnetic field direction,

$$\mathbf{z}_{\pm} \perp \mathbf{B}_0, \quad |\nabla_{\parallel} \mathbf{z}_{\pm}| \ll |\nabla_{\perp} \mathbf{z}_{\pm}|. \quad (5)$$

Transverse fluctuations are assumed to be of the incompressible type, so $\nabla_{\perp} \cdot \mathbf{z}_{\pm} = 0$, with respect to the local or fast coordinate, although background density ρ can vary in the large scale.

Theory and simulations indicate that in the presence of a sufficiently strong mean field or for sufficiently small plasma beta, three-dimensional compressible MHD dynamically reorganizes to favor RMHD-type fluctuations (Zank & Matthaeus 1992; Matthaeus et al. 1996a, 1998; Oughton, Priest, & Matthaeus et al. 1994; Kinney & McWilliams 1998; Oughton, Ghosh, & Matthaeus 1998). The corona is a suitable example of a low-beta plasma, and therefore RMHD has been successfully employed in models and simulations of coronal heating (Longcope & Sudan 1994; Hendrix & van Hoven 1996; Dmitruk & Gómez 1999; Oughton et al. 2001).

We will indicate by s the coordinate on the parallel direction where fields vary slowly. This variable can be a Cartesian coordinate or a radial coordinate, depending on the

geometry assumed. The mean magnetic field and therefore the Alfvén velocity is in this direction, $V_A = V_A(s)\hat{s}$.

Under these considerations, equations (4) take the form

$$\begin{aligned} \frac{\partial \mathbf{z}_{-}}{\partial t} + V_A \frac{\partial \mathbf{z}_{-}}{\partial s} + \frac{1}{2} \nabla \cdot V_A (\mathbf{z}_{+} - \mathbf{z}_{-}) - \frac{\mathbf{z}_{+}}{\sqrt{4\pi\rho}} \cdot \nabla \mathbf{B}_0 \\ = -\frac{1}{\rho} \nabla_{\perp} p - \mathbf{z}_{+} \cdot \nabla_{\perp} \mathbf{z}_{-} + \mathbf{D}_{-} \\ \frac{\partial \mathbf{z}_{+}}{\partial t} - V_A \frac{\partial \mathbf{z}_{+}}{\partial s} + \frac{1}{2} \nabla \cdot V_A (\mathbf{z}_{+} - \mathbf{z}_{-}) - \frac{\mathbf{z}_{-}}{\sqrt{4\pi\rho}} \cdot \nabla \mathbf{B}_0 \\ = -\frac{1}{\rho} \nabla_{\perp} p - \mathbf{z}_{-} \cdot \nabla_{\perp} \mathbf{z}_{+} + \mathbf{D}_{+}, \end{aligned} \quad (6)$$

where we have explicitly expressed the nonlinear terms N_L for the RMHD approximation on the right-hand side of the equations.

The left-hand side of the equations contains only linear terms. The second term represents propagation of fluctuations with Alfvén velocity, i.e., Alfvén waves. In our notation \mathbf{z}_{-} propagates upward (from the Sun's surface) and \mathbf{z}_{+} propagates downward. The other linear terms on the left-hand side represent reflections due to the inhomogeneities of the background medium. An initial population of upward waves can give rise to a "reflected" population of downward waves owing to the presence of these terms. This effect is entirely analogous to the what has been called a "mixing" effect (Zhou & Matthaeus 1990) in transport equations developed for solar wind turbulence (see also Marsch & Tu 1993; Tu & Marsch 1989). The main difference between the two cases is that in the corona the large-scale (wind) speed U is presumably much smaller than the Alfvén speed V_A . Thus terms of $O(U/V_A)$ have been neglected in writing equation (6). On the other hand in the outer heliosphere the opposite inequality $V_A/U \ll 1$ is reasonably well satisfied, and many features of solar wind transport can be understood neglecting terms involving the Alfvén speed (Matthaeus et al. 1999b). An additional distinction is that both fluctuation types, \mathbf{z}_{+} and \mathbf{z}_{-} , are transported outward in the super-Alfvénic wind, and the transport problem becomes a one-point boundary value problem. In the corona the propagation of fluctuations is in both directions, and the transport problem becomes a two-point boundary value problem.

For the coronal problem the background profiles of Alfvén velocity, magnetic field, and density determine the coefficients of the linear terms, and they can be complicated functions of the slow coordinate s . The study of linear Alfvén waves in nonhomogeneous media has been done extensively in the past (Hollweg 1981, 1984, 1996; Heinemann & Olbert 1980; An et al. 1989, 1990; Moore et al. 1991; Velli 1993) using different one-dimensional (usually radial) profiles. In some cases, the linear equations can be reduced to the Klein-Gordon form (Musielak, Fontenia, & Moore 1992), and so dispersive waves solutions are obtained, with evanescent and resonant type of phenomena, according to the relation between the frequency of a wave forcing imposed and the reflection coefficient of the medium.

On the right-hand side of equations (6) we placed the nonlinear terms. Since they are always neglected in the linearized studies mentioned before, our goal here is to include

them in the description. A first inspection of the form of the nonlinear terms shows they are trivially zero unless both upward and downward fluctuations are present. As mentioned before, reflections provide a way to generate downward fluctuations from an initially upward population of fluctuations, so they are essential for the development of turbulence.

A complete simulation of equations (6), with exact treatment of the nonlinear terms, is presented in a further publication (Dmitruk et al. 2001) where the conditions for the actual development of turbulence are studied. As an alternative way to look into the problem, we extend here the model introduced by Matthaeus et al. (1999a), adopting a similar phenomenological description of the nonlinear terms. Despite its simplifications, our model can provide insight into the physics of the problem and specifically into the understanding of the interaction between propagation, reflection and nonlinear effects, and their spatial dependence. The model also turns out to be very useful to perform parameter variation studies that are computationally costly in a direct numerical simulation of the full RMHD equations.

Our aim is to develop a model for the evolution of the perpendicular fields z_{\pm} with the following properties:

1. An exact description of the propagation and reflection terms (“ s -dependence”).
2. A phenomenological, simplified description of the nonlinear terms.
3. More realistic boundary conditions in “ s .”
4. Only large scales of the fluctuations will be considered in perpendicular planes.

By “large scales” in the perpendicular planes we mean scales of the order of the transverse size of the domains considered, which in a coronal situation correspond to the inter-network length. This typical size is still much smaller than variations in the vertical direction (of the order of a solar radius), which is consistent with the RMHD ordering.

Property 1 establishes one of the main differences with the s -averaged model presented in Matthaeus et al. (1999a). Property 2 implies, for a coronal MHD scenario,

$$D^{\pm} = 0 \quad (7)$$

since the molecular viscosity and resistivity give place to typical dissipation times, which are exceedingly large when the dissipation operator acts on the large scales.

On the other hand, the reflections will favor the production of counterpropagating waves, which in turn will excite a very strong nonlinear state. This nonlinear state is likely to be turbulent, with a direct cascade of energy to small scales, in perpendicular planes. In such scenario, it is expected that the nonlinear terms will represent to the large scales a continuous energy drag. If we assume an independent two-dimensional Kolmogorov-like turbulent state at each plane $s = \text{constant}$, a phenomenological turbulent dissipation rate can be expressed as (Matthaeus et al. 1999a; Hossain et al. 1995)

$$\left. \frac{d(Z_-^2 + Z_+^2)}{dt} \right|_{\text{turb diss}} = - \frac{Z_-^2 Z_+ + Z_+^2 Z_-}{\lambda_{\perp}}, \quad (8)$$

where Z_{\pm}^2 are the spatial two-dimensional averages of z_{\pm}^2 at each perpendicular plane and $Z_{\pm} \equiv \sqrt{Z_{\pm}^2}$. The basic structure of the cross helicity-dependent nonlinear terms

employed above derives in large part from the structure of earlier one-point phenomenological treatments (Dobrowolny, Mangeney, & Veltri 1980) and two-point closure theories (Grappin et al. 1982) for MHD turbulence. In this expression, λ_{\perp} is a similarity length scale associated with the energy decay, such as that which appears in hydrodynamic turbulence closures (e.g., von Kármán & Howarth 1938; Matthaeus, Zank, & Oughton 1996b). However in view of the anisotropic cascade, this length scale is associated with the transverse structure of the fluctuations. Here we assume that λ_{\perp} may be approximated as a length scale representative of the transverse dimensions of the energy containing turbulent eddies. In the practical sense this means λ_{\perp} would be of the order of magnitude of the correlation length (Matthaeus et al. 1999a), which is an observable quantity that we identify with the inter-network scale at the coronal base. Anticipating a near steady state, we take λ_{\perp} here to be a constant.

Ultimately, the precise value of λ_{\perp} must be determined by comparisons to simulations that consider the exact nonlinear terms. In a way, λ_{\perp} can be thought of as the tuning parameter of the phenomenological model, since it may incorporate overall multiplicative constants in relations such as equation (8) (see, e.g., Matthaeus et al. 1996b).

Motivated by the structure of equation (8), we may ask how a model term may be constructed to represent the effects of turbulence in the more primitive equations for the fluctuations themselves, such as equation (6). In this regard we propose the following model for the nonlinear terms:

$$N_L^{\pm} = -z_{\mp} \cdot \nabla_{\perp} z_{\pm} \approx - \frac{Z_{\mp}}{2\lambda_{\perp}} z_{\pm}. \quad (9)$$

Note that this model provides a turbulent heating rate consistent with equation (8), as it can be readily verified by computing the two-dimensional average of $2z_+ \cdot N_L^+ + 2z_- \cdot N_L^-$. Note that equation (9) can be thought as an approximation in which the $z_{\mp} \cdot \nabla$ operator is modeled as a simple dragging coefficient $Z_{\mp}/2\lambda_{\perp}$. Note that in equation (6) the left-hand side is entirely insensitive to the structure of the fluctuation in the directions transverse to the large-scale magnetic field. Thus, once the above model for the turbulence is inserted as a replacement for the terms on the right-hand side of equation (6), the transverse structure is simply a label in each term. (One should keep in mind of course that the cascade in reality depends crucially on the transverse structure.) This provides us with considerable flexibility in how we may average over or filter transverse structure, provided that we continue to employ a proper nonlinear model. We may imagine for example that the turbulence consists of a “gas” of Fourier modes, each one of which interacts with very many of the others. However if we may make the bold assumption that our very simple model for the nonlinear effects of the cascade is adequate, we may think of the effects of all other Fourier modes on any one of them as being represented by this simple term. We may then focus on any one large-scale energy-containing mode of the system as being representative and compute its evolution under the combined effects of the (linear) propagation and reflection terms, and the nonlinear cascade terms modeled as in equation (9). Thus we seek solutions of the form

$$z_{\pm} = z_{\pm}(s, t) \cos(kx)\hat{x}, \quad (10)$$

where $k = 2\pi/l$ and l is the transverse size of the system. In this case, $Z_{\pm} = |z_{\pm}|$ and the equations (6) reduce to

$$\frac{\partial z_-}{\partial t} = -V_A(s) \frac{\partial z_-}{\partial s} - R_1(s)z_+ + R_2(s)z_- - \frac{z_- |z_+|}{2\lambda_{\perp}} \quad (11)$$

$$\frac{\partial z_+}{\partial t} = V_A(s) \frac{\partial z_+}{\partial s} + R_1(s)z_- - R_2(s)z_+ - \frac{z_+ |z_-|}{2\lambda_{\perp}}. \quad (12)$$

The reflection rates (with dimension 1/time) are

$$R_1(s) = R_2(s) = R(s) = \frac{1}{2} \frac{dV_A}{ds} \quad (13)$$

in the case of a Cartesian coordinate, or

$$R_1(r) = \frac{1}{2} \frac{dV_A}{dr} \quad (14)$$

$$R_2(r) = \frac{1}{2} \frac{dV_A}{dr} + \frac{V_A}{r} \quad (15)$$

for a radial $s = r$ coordinate in spherical geometry.

Different Alfvén velocity and consistent reflection profiles can be assumed. We worked mainly with mathematically smooth profiles in planar geometry, with the general characteristics of a realistic coronal situation. Several results with different kind of values for profiles properties are considered. Cases using radial profiles such as those employed by previous authors in linear studies (An et al. 1990; Velli 1993) will be studied in the future.

Equations (11) and (12) must be completed with adequate boundary conditions. Characteristics of these equations are given by the solutions of the equation $ds/dt = V_A(s)$ in the plane (s, t) . In-going characteristics at $s = 0$, i.e., the bottom boundary, are prescribed for the z_- field, and in-going characteristics at $s = 1$ (in adimensional units), i.e., the top boundary, are prescribed for the z_+ field. A given function of t for the fields or combination of fields and its first derivatives can be imposed at the boundaries. Initial conditions at $t = 0$ for all the s -domain considered must also be given. The problem is of the initial boundary value type. We assume zero initial fields, and the following boundary conditions:

$$z_-(s = 0, t) = A_{\text{in}} \sin(2\pi ft) \quad (16)$$

$$z_+(s = 1, t) = 0. \quad (17)$$

This represents a monochromatic wave-forcing function, with frequency f and amplitude A_{in} . The effect of different values for f is presented in the parameter variation studies section. For the top boundary, no inward fluctuations are allowed to enter the box. This guarantees that all reflections are generated within the domain considered and are due to the inhomogeneities of the medium. This is a fairly conservative approach, since a certain level of inward fluctuations might be present at about $2 R_{\odot}$. Nonetheless, we choose to study only self-generated inward fluctuations.

2.1. Energy Balance and Heating Efficiency

We will now obtain energy balance relations from equations (11) and (12). The expressions below apply to planar (Cartesian) geometry, but similar results can be readily obtained for radial geometry (providing the correct radial

dependence of the mean magnetic field and volume factors are included in the integrals).

The energies of the fluctuating fields are defined as

$$E_{\pm} = \frac{1}{4} \int \rho z_{\pm}^2 d^3x. \quad (18)$$

We can relate the density with the Alfvén velocity, using

$$V_A = \frac{B_0}{\sqrt{4\pi\rho}} \quad (19)$$

$$\mathbf{B}_0 = B_0(s)\hat{s}, \quad \nabla \cdot \mathbf{B}_0 = \frac{\partial B_0}{\partial s} = 0, \quad (20)$$

which implies

$$V_A^2 \rho = \text{constant} \rightarrow \rho = \frac{V_{A_0}^2}{V_A^2} \rho_0, \quad (21)$$

where V_{A_0}, ρ_0 are the values at the bottom boundary. We further define the energy per unit mass as

$$\langle z_{\pm}^2 \rangle = \frac{E_{\pm}}{\rho_0 V} = \frac{1}{4V} \int \frac{V_{A_0}^2}{V_A^2} z_{\pm}^2 d^3x, \quad (22)$$

where V is the volume of the domain under consideration. The averaging operation $\langle \cdot \rangle$ will mean hereafter averaging over the volume V with a weight factor $V_{A_0}^2/V_A^2$.

In order to find evolution equations for the energies, we multiply equation (11) by $(V_{A_0}^2/V_A^2)z_-$ and equation (12) by $(V_{A_0}^2/V_A^2)z_+$ and use the following identity to cancel diagonal reflection terms (see eq. [13]):

$$\frac{1}{2V_A} \frac{\partial z^2}{\partial s} = \frac{\partial}{\partial s} \left(\frac{z^2}{2V_A} \right) + \frac{1}{2} \frac{dV_A}{ds} \frac{z^2}{V_A^2} = \frac{\partial}{\partial s} \left(\frac{z^2}{2V_A} \right) + R_1(s) \frac{z^2}{V_A^2}. \quad (23)$$

After averaging we obtain

$$\frac{d}{dt} \langle z_-^2 \rangle = F_-^{\text{bot}} - F_-^{\text{top}} - 2\langle R z_+ z_- \rangle - \frac{\langle z_-^2 | z_+ | \rangle}{\lambda_{\perp}} \quad (24)$$

$$\frac{d}{dt} \langle z_+^2 \rangle = F_+^{\text{top}} - F_+^{\text{bot}} + 2\langle R z_+ z_- \rangle - \frac{\langle z_+^2 | z_- | \rangle}{\lambda_{\perp}}, \quad (25)$$

where the fluxes are defined as

$$F_{\pm} = \frac{1}{4} \frac{V_{A_0}^2}{L_s} \frac{z_{\pm}^2}{V_A} \quad (26)$$

(L_s is the vertical size of the domain considered). According to the boundary conditions assumed, $F_+^{\text{top}} = 0$, i.e., no energy flux enters through the top boundary. The energy flux of upward fluctuations at the bottom is

$$F_-^{\text{bot}} = \frac{1}{4} \frac{V_{A_0}}{L_s} A_{\text{in}}^2 \sin^2(2\pi ft), \quad (27)$$

where A_{in} is the imposed amplitude of the forcing wave. The net flux of energy at the bottom boundary, $F_-^{\text{bot}} = F_-^{\text{bot}} - F_+^{\text{bot}}$, depends, however, on the response of the system, since F_+^{bot} is not prescribed by the boundary conditions and is given by the dynamics of reflections and nonlinearities within the domain. The net energy flux entering the corona is usually expressed as energy per unit time per unit area, in

which case this corresponds to

$$F_0 = \rho_0 L_s F^{\text{bot}} = \rho_0 L_s V_{A_0} \left(\frac{z_-^2 - z_+^2}{4} \right)^{\text{bot}}. \quad (28)$$

A typical range (Withbroe & Noyes 1977) of coronal values in open field line regions is $F_0 \sim (5 \times 10^5) - (8 \times 10^5)$ ergs $\text{cm}^{-2} \text{s}^{-1}$.

The energy flux of upward fluctuations at the top, F^{top} represents an energy transmission rate, i.e., energy that goes away and is not dissipated as heating within the domain.

The reflection terms are of the opposite sign in each energy equation, and they are conservative, in the sense that they cancel each other when the total energy balance is computed. The total energy balance is obtained after the sum of equations (24) and (25):

$$\frac{d}{dt} (\langle z_-^2 \rangle + \langle z_+^2 \rangle) = F^{\text{bot}}(t) - F^{\text{top}}(t) - \epsilon(t), \quad (29)$$

where $\epsilon(t)$ represents the phenomenological turbulent dissipation rate and determines the heating within the box,

$$\epsilon(t) = \frac{\langle z_-^2 | z_+ | \rangle}{\lambda_\perp} + \frac{\langle z_+^2 | z_- | \rangle}{\lambda_\perp}. \quad (30)$$

In equations (29)–(30) we explicitly noted the time dependence of quantities such as the heating rate, or the flux at the boundaries. Indeed, the system does not reach a strictly steady state but evolves to a time-periodic state, with period τ given by the inverse of the forcing frequency, f . Thus, the left-hand side of equation (29) vanishes after a forcing period time average, yielding

$$\bar{F}^{\text{bot}} = \bar{F}^{\text{top}} + \bar{\epsilon}, \quad (31)$$

where $\bar{\epsilon} = (1/\tau) \int \epsilon(t) dt$, and $\bar{F}^{\text{bot, top}} = (1/\tau) \int F^{\text{bot, top}}(t) dt$. Most of the results presented in the next section will be this type of time average, computed after the system reaches an oscillatory steady state.

Equation (31) express the fact that the injected energy at the bottom is (in time average) either dissipated by turbulence or transmitted at the top. The efficiency of the turbulence is defined as the ratio between the turbulent dissipation rate and the net energy flux entering through the bottom boundary

$$\gamma = \bar{\epsilon} / \bar{F}. \quad (32)$$

The fraction of the flux transmitted away from the domain is $1 - \gamma$.

Another useful quantity is the normalized cross helicity

$$\sigma_c(t) = \frac{\int (z_+^2 - z_-^2) ds}{\int (z_+^2 + z_-^2) ds}, \quad (33)$$

which measures the amount of counterpropagating waves. For a single population of upward waves, $\sigma_c = -1$, but this value may increase up to 0, which is the case when equipartition between upward and downward fluctuations exists.

It is interesting to investigate the role of the correlation $\langle R z_+ z_- \rangle$, which appears on the right-hand side of equations (25)–(24), and represents the effect of the reflections in the energies of the fields. This correlation does not contribute to the total energy, but it redistributes the energy between z_+ and z_- . Operating with equations (11)–(12) we

obtain

$$\begin{aligned} \frac{d}{dt} \langle R z_+ z_- \rangle &= \left\langle V_A R \left(z_- \frac{\partial z_+}{\partial s} - z_+ \frac{\partial z_-}{\partial s} \right) \right\rangle \\ &+ \langle R^2 (z_-^2 - z_+^2) \rangle - \frac{\langle (|z_+| + |z_-|) R z_+ z_- \rangle}{2\lambda_\perp}. \end{aligned} \quad (34)$$

The second term on the right-hand side of equation (34) tends to produce equipartition between the z_\pm fields, thus reducing cross helicity, as can be seen by inspection of equations (25)–(24). The third term on the right-hand side of equation (34), on the other hand, acts as a dissipation for the $\langle R z_+ z_- \rangle$ correlation and is thus opposite to the effect of the second term. Both effects thus compete, as it is further discussed in § 3.2

2.2. Adimensional Equations

The dynamical equations of the problem (eqs. [11] and [12]) are solved numerically using a Chebyshev collocation method for the s -derivatives and explicit second-order time integration. We adopt $L_s = R_\odot$ as the length unit in the propagation direction s , in a domain of height R_\odot (i.e., $s \in [0, 1]$) measured from the coronal base. It is assumed that this length is representative of the order of magnitude of scale height variations of typical Alfvén velocity profiles. The unit of time is chosen to be $t_{A_0} = R_\odot / V_{A_0}$, where V_{A_0} is the Alfvén velocity at the coronal base. This is of the order of magnitude of the Alfvén wave crossing time over the domain in s , which depends on the Alfvén velocity profile adopted. Fluctuating fields are measured in velocity units, and we employed a unit z_0 related to the heating flux expression (eq. [28]), $z_0 = (F_0 / \rho_0 V_{A_0})^{1/2}$. The adimensional version of the dynamical equations (eqs. [11] and [12]) is

$$\frac{\partial z_\mp}{\partial t} = \mp \tilde{V}_A \frac{\partial z_\mp}{\partial s} \mp \tilde{R} z_\pm \pm \tilde{R} z_\mp - \eta_{\text{eff}} \frac{z_\mp |z_\pm|}{2}, \quad (35)$$

where $\tilde{V}_A(s) = V_A(s) / V_{A_0}$, $\tilde{R}(s) = \frac{1}{2} d\tilde{V}_A / ds$ and

$$\eta_{\text{eff}} = \frac{z_0}{V_{A_0}} \frac{R_\odot}{\lambda_\perp} = \frac{\sqrt{F_0 / \rho_0} V_{A_0}}{V_{A_0}} \frac{R_\odot}{\lambda_\perp}. \quad (36)$$

Note that the dimensional equations (eqs. [11]–[12]) can be formally transformed to the dimensionless equations (eq. [35]) by identifying

$$V_A \leftrightarrow \tilde{V}_A, \quad R \leftrightarrow \tilde{R}, \quad \frac{1}{\lambda_\perp} \leftrightarrow \eta_{\text{eff}}. \quad (37)$$

In the following sections we present results of numerical solutions of equation (35) for different types of Alfvén velocity profiles, parameters, and forcing.

3. RESULTS AND DISCUSSION

3.1. Alfvén Profile Properties

We have chosen for a first set of simulations a mathematically smooth Alfvén velocity profile, which increases from $V_{A_0} \approx 1000 \text{ km s}^{-1}$ to $V_{A_{\text{MAX}}} \approx 4000 \text{ km s}^{-1}$ over a distance of $1 R_\odot$ from the coronal base. This profile and the associated reflection coefficient rate, $R = \frac{1}{2} (dV_A / ds)$, are shown in Figure 1. Reflection is exactly zero at boundaries and has a maximum at the midpoint of the domain. The variation of the Alfvén velocity ΔV_A over the domain can be

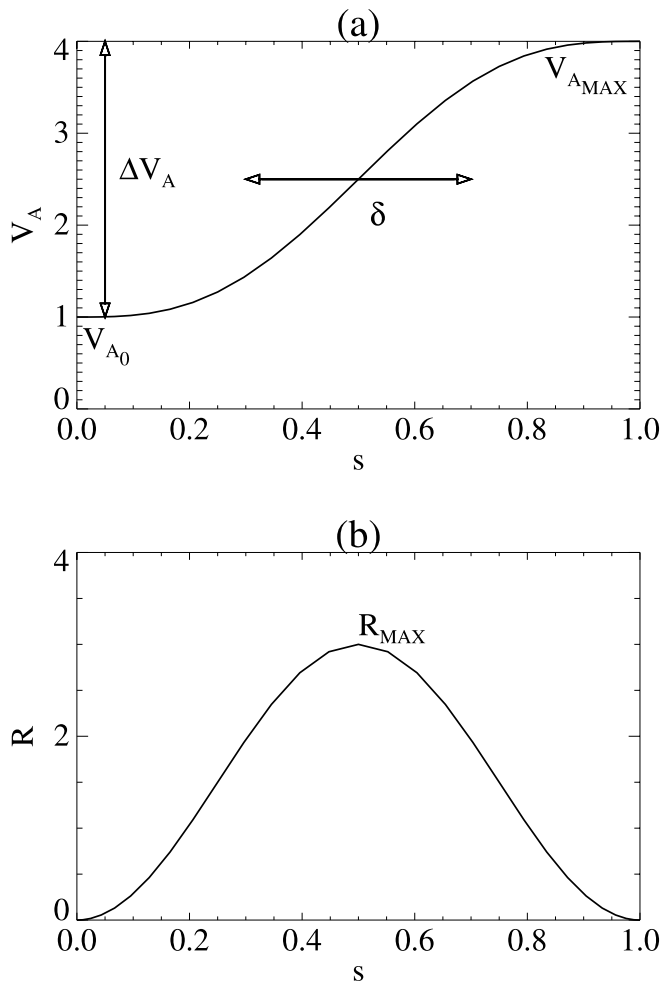


FIG. 1.—(a) Typical Alfvén velocity profile employed; velocity is measured in units of $V_{A0} = 10^3 \text{ km s}^{-1}$. (b) The corresponding reflection coefficient rate, in units of $1/t_{A0} = 1/700 \text{ s}^{-1}$.

increased, and this will increment the value of the reflection coefficient. However this change also increases the overall effect of the propagation term, since Alfvén velocities will be higher. A measure of the weight of reflections over propagation can then be expressed by the ratio $\Delta V_A/V_{A MAX}$.

The effect of changing this ratio on the overall steady heating efficiency γ and the time-averaged normalized cross helicity σ_c is shown in Figure 2a, corresponding to a case with $\eta_{eff} = 0.6$ and frequency (in $1/t_{A0}$ units) $f = 0.1$. It is clear that no heating is obtained when ΔV_A is 0, since in this case there are no reflections, as can also be seen from the fact that $\sigma_c = -1$. A slow increase in the Alfvén velocity difference is enough to turn on reflections and produce a sustained heating. The efficiency increases nonlinearly as the normalized gradient of the Alfvén velocity is higher.

Another possible change in the Alfvén velocity profile is to increase the steepness, keeping constant the total increase of Alfvén speed. The steepness is measured by the ratio δ/L_s , where δ (see Fig. 1) is the scale height over which an appreciable change in the Alfvén velocity occurs. The effect of this variation is shown in Figure 2b, for the same η_{eff} and f as in the previous case, and keeping $\Delta V_A/V_{A MAX} = \frac{3}{4}$. There is almost no change of efficiency or cross helicity. The reason for that is that even though the steepness of the profile increases the maximum value of reflection achieved, the

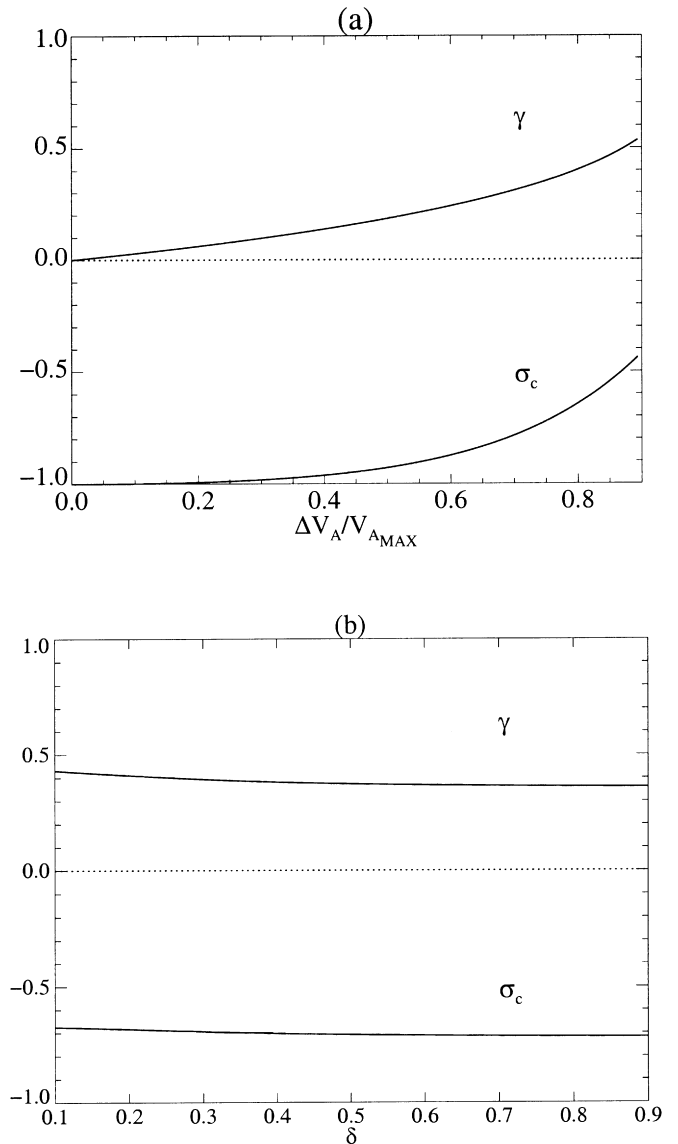


FIG. 2.—Efficiency and helicity (time-averaged) as a function of (a) ratio of total Alfvén velocity increase/ maximum Alfvén velocity and (b) scale height length δ (steepness of the Alfvén velocity profile) with fixed ratio $\Delta V_A/V_{A MAX} = \frac{3}{4}$. In both plots $\eta_{eff} = 0.6$ and the forcing frequency $f = 0.1$

value of the reflection in the rest of the domain will be lower, and the average effect will be the same (provided the step ΔV_A is kept constant) as in the smooth profile case.

3.2. Phenomenological Parameter Dependence

The value of η_{eff} is determined by (1) the physical values of observable quantities as the flux in the boundary, density, and Alfvén velocity, and (2) the length scale λ_{\perp} representative of the transverse dimensions of the energy-containing eddies which is of the order of magnitude of the internetwork distance at the coronal base, as we mentioned before, but its precise value must be tuned with simulations including the exact nonlinear terms. We will investigate such a comparison of direct turbulence simulation with the present phenomenology in a future work. Previously we have found that phenomenological heating rates compare reasonably well in direct simulation studies (Hossain et al. 1995) and give qualitatively similar results for a periodic RMHD coronal wave heating model (Oughton et al. 2001).

A possible range of values for the physical parameters relevant to an open field line region of the lower corona is $F_0 \sim 10^5\text{--}10^6$ ergs cm^{-2} s^{-1} for the energy input flux, $V_{A0} \sim 10^3$ km s^{-1} for the Alfvén velocity, and $\rho_0 = m_p n_0$ for the mass density, with m_p the proton mass and $n_0 \sim 10^8$ cm^{-3} the coronal number density. The inter-network distance at the coronal base is $\sim 30 \times 10^3$ km and possibly an order of magnitude lower. This renders a range of possible values of $\eta_{\text{eff}} \sim 0.3\text{--}20$.

Note that η_{eff} is a measure of the relevance of the nonlinear transverse cascade, as it is clear from equation (35). It is therefore very instructive to study the parametric dependence of the solutions of our equations on η_{eff} . Figure 3 shows the dependence of the heating efficiency and time-averaged normalized cross helicity, as a function of η_{eff} . In this case, $\Delta V_A/V_{A\text{MAX}} = \frac{3}{4}$ and the forcing frequency $f = 0.1$. We extend the range of possible values of η_{eff} to study the asymptotic behavior of the solutions. The asymptotic cases $\eta_{\text{eff}} \gg 1$ and $\eta_{\text{eff}} \ll 1$ can be understood, as follows. When η_{eff} goes to zero, the nonlinear turbulent dissipation becomes negligible. As a consequence, the efficiency of the model tends to zero, as shown in the figure. Also, it is expected that in this limit the correlations $\langle R z_+ z_- \rangle$ will not be attenuated by dissipation (see discussion at the end of § 2.1), and the reflected fluctuations z_+ will be comparable to z_- , thus yielding a value of σ_c significantly larger than -1 , which is consistent with Figure 3.

The other limit, $\eta_{\text{eff}} \gg 1$, is also interesting. Note that in this case the $\langle R z_+ z_- \rangle$ term is strongly damped by the third term in the right-hand side of equation (34), as discussed before, and will not produce any significant transfer of energy from z_- to z_+ . As a result, $(z_+/z_-) \rightarrow 0$, implying $\sigma_c \rightarrow -1$, as it is shown in Figure 3. The asymptotic behavior of the heating efficiency is nontrivial in this limit. Applying equation (37) to equation (30), and neglecting the term $O(z_+^2)$, we see that the nondimensional dissipation rate tends to

$$\tilde{\epsilon}(t) = \eta_{\text{eff}} \langle z_-^2 | z_+ | \rangle. \quad (38)$$

While $|z_+| \rightarrow 0$ and $\eta_{\text{eff}} \rightarrow \infty$, the product $\eta_{\text{eff}} |z_+|$ remains finite, resulting in a finite value for the heating efficiency, as

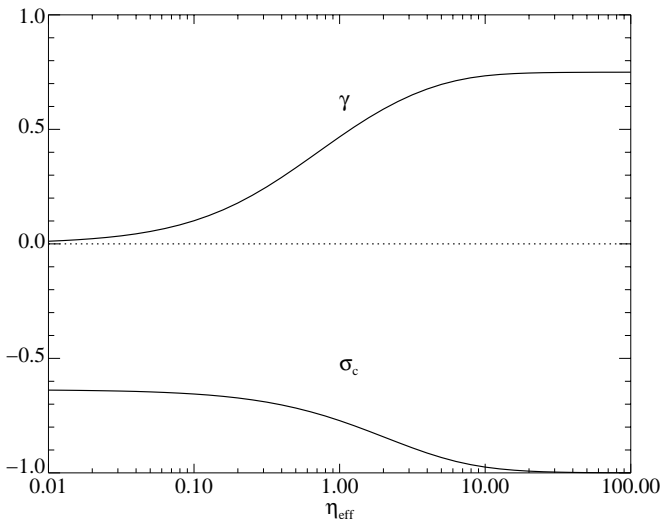


FIG. 3.—Efficiency and helicity (time-averaged) as a function of η_{eff} , the parameter in the phenomenological nonlinear term. In this case $\Delta V_A/V_{A\text{MAX}} = \frac{3}{4}$ and $f = 0.1$.

we immediately show. We begin expanding equation (35) for $\partial z_+/\partial t$ to first order in the small ratio (z_+/z_-) (assuming $z_- \neq 0$), to obtain

$$\eta_{\text{eff}} z_+ = 2\tilde{R} \frac{z_-}{|z_-|}. \quad (39)$$

As we anticipated, $\eta_{\text{eff}} |z_+|$ tends to a finite limit. It is remarkable that in this limit the vertical fluctuation profile $z_+(s)$ reproduces exactly the reflection rate profile $\tilde{R}(s)$ (apart from a scaling factor $2\eta_{\text{eff}}^{-1}$). We now expand equation (35) for $\partial z_-/\partial t$, and replace equation (39) in the nonlinear term, which happens to cancel with the diagonal reflection term, yielding

$$\frac{\partial z_-}{\partial t} = -\tilde{V}_A \frac{\partial z_-}{\partial s}. \quad (40)$$

After time averaging over a forcing period, and using periodicity, we obtain $\tilde{V}_A(\partial/\partial s)\bar{z}_-^2 = 0$. That is, the time-averaged amplitude of the z_- fluctuations is uniform in s . This property, together with equation (39), simplifies the computation of the time-averaged heating rate on equation (38), and the heating efficiency takes the simple form

$$\gamma \rightarrow \frac{\Delta V_A}{V_{A\text{MAX}}} \quad \text{when } \eta_{\text{eff}} \rightarrow \infty. \quad (41)$$

Note that, in general, for finite η_{eff} , the evaluation of the spatial average in equation (38) cannot be performed a priori. However, we may study numerically the efficiencies and their approach to the asymptotic $\eta_{\text{eff}} \rightarrow \infty$ state. Figure 3 corresponds to an Alfvén profile in which $\Delta V_A/V_{A\text{MAX}} = \frac{3}{4}$, which is the asymptotic value of the efficiency shown in the figure. A set of different numerical solutions for increasing values of η_{eff} is shown in Figure 4. The efficiency γ is plotted as a function of $\Delta V_A/V_{A\text{MAX}}$. It can be noticed that the asymptotic limit of equation (41), which corresponds to a line of slope 1, is reached for values of $\eta_{\text{eff}} > 20$, which is not too high, given the possible observational range of values for this parameter (see above).

3.3. Forcing Frequency Dependence

The effect of the variation of the wave-forcing frequency f (see eq. [16]) is shown in Figure 5. The other parameters

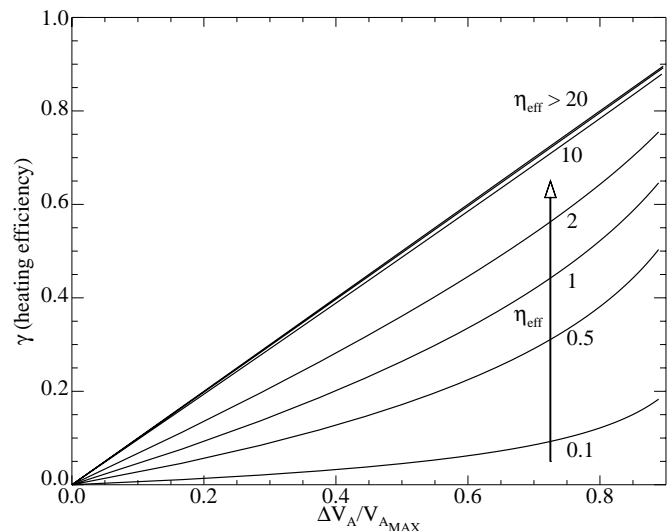


FIG. 4.—Efficiency as a function of $\Delta V_A/V_{A\text{MAX}}$ for increasing values of η_{eff} . The line of slope 1 correspond to the asymptotic limit for $\eta_{\text{eff}} \rightarrow \infty$.

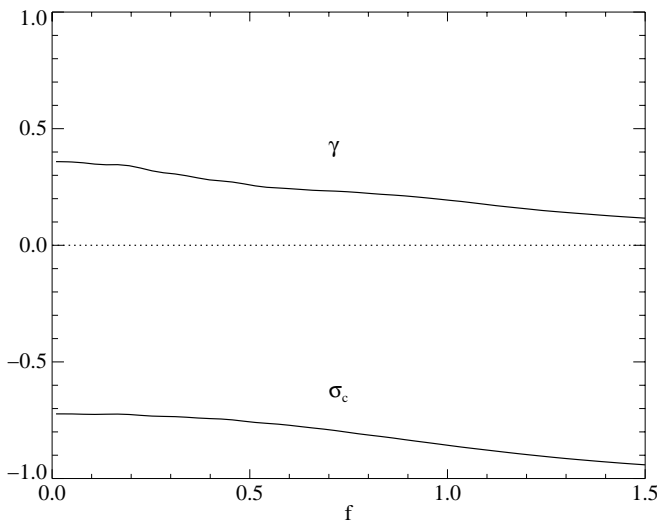


FIG. 5.—Efficiency and helicity as a function of the wave-forcing frequency f ; the value $f = 1$ corresponds to a forcing period = t_{A_0} , the Alfvén time. For this solution, $\eta_{\text{eff}} = 0.6$ and $\Delta V_A/V_{A_{\text{MAX}}} = \frac{3}{4}$.

have been fixed at $\eta_{\text{eff}} = 0.6$ and $\Delta V_A/V_{A_{\text{MAX}}} = \frac{3}{4}$ for this study. As it can be seen in the figure, the dissipation efficiency of the system decreases with increasing frequency.

This result provides considerable insight into the role of wave frequency in turbulent coronal heating. Parker (1991) has taken the position that quasi-static motions of photospheric field lines are a more effective way to heat the corona than high-frequency waves would be. In his view, quasi-static motions compel the formation of current sheet structures which greatly enhance dissipation rates. In our units, waves with frequency $f = 1$ correspond to a forcing period of t_{A_0} , the approximate Alfvén wave crossing time over the domain. Quasi-static motions at the coronal base correspond to the case $f \ll 1$. We see then that Parker’s point is born out in our solutions, in that the efficiency γ is greatest when $f \rightarrow 0$. However, the results also show that the cascade is only modestly suppressed when driven by frequency waves $f \approx 1$. Another recent examination of coronal cascade driven by reflected waves (Oughton et al. 2001) has shown that the mode of dissipation in the steady cascade is through formation of thin current sheets and turbulent reconnection as suggested by Parker. However, it appears that frequency waves ($f \approx 1$) can excite the same sort of cascade, though somewhat less efficiently than when driven by quasi-static driving $f \ll 1$.

Moving toward higher frequencies, we see a general decrease of efficiency. Although we cannot justify the use of an RMHD model for truly high frequency waves $f \gg 1$, we can view the general monotonic downward trend of $\gamma(f)$ as suggestive of the inefficiency of driving a cascade in this way through injection of high-frequency waves at the coronal base. Models that rely upon a flux of high-frequency waves (Axford & McKenzie 1997; Cranmer et al. 1999; Tu & Marsch 1997) generally argue that direct kinetic damping effects are the dominant associated dissipation channel. The present result does not contradict this and moreover suggests that turbulent cascade will not be an effective supplement to these effects. The same conclusion has been suggested previously as a consequence of cascade anisotropy (Leamon et al. 2000).

Study of the relative importance of high-frequency or low-frequency processes for the heating would need an

expression for the frequency spectrum of the forcing. Our forcing function is monochromatic for simplicity. But in general, the forcing is expected to have a whole range of frequencies. Several factors in the network and chromosphere may favor the importance of a low-frequency energy source for coronal heating. First, one might think that the spectrum of strongly nonlinear activity in the network itself is initially decreasing with frequency, as most turbulence spectra decrease (overall) with both frequency and wavenumber. Second, MHD studies show that cascade in parallel wave vector (wave frequency cascade for Alfvén waves) is inhibited (Leamon et al. 2000). Thus, turbulence cascade tends to occur at low relatively fixed wave frequency. Third, the present result is that heating efficiency monotonically decreases with forcing frequency. On the other hand, there is one factor, perhaps a strong one, that disfavors low frequencies. That is, lower frequency waves should have relatively greater difficulty in getting through the transition region and into the corona (Hollweg 1981, 1984). Further studies that include chromospheric and transition region effects will be needed to clarify this situation. Indeed, recent MHD simulations (Kudoh & Shibata 1999) that employ broadband wave spectral input at the photospheric boundary find that adequate wave power to heat the corona ($\sim 3 \times 10^5 \text{ ergs cm}^{-2} \text{ s}^{-2}$) is transported through the transition region. The resulting coronal frequency spectra are more-or-less monotonically decreasing in frequency. This suggests the presence of adequate low-frequency power to drive a cascade such as that which we envision here. If this result is maintained, it would seem to support both the present model and Parker’s model in that the lowest frequency waves that survive the transition region should be effective in driving the cascade and heating in the corona.

It also has to be noted that recent observations allowed Mandrini, Démoulin, & Klimchuk (2000) to compare empirical scaling laws in coronal loops with the scaling laws derived from many coronal heating models, finding an overall better agreement with the quasi-static models, rather than the wave-heating models, although their study has not been done for open field line regions such as the one we considered here.

3.4. Behavior of the Solutions in s

An interesting aspect of this model is the possibility to study the behavior of the system along the propagation direction s . An important point in heating models of the solar wind is that most of the heating actually occurs in the first fraction of solar radius from the Sun’s surface. This is also related to models of acceleration of the wind (McKenzie et al. 1995; Habbal et al. 1995; Evje & Leer 1998) in which a “dissipation length,” associated with an ad hoc heat deposition mechanism, is invoked to provide needed heating and pressure to drive the acceleration of the wind. We can easily demonstrate that the present model provides a framework in which the dissipation mechanism, identified as that due to cascade and turbulence, plays the required role of deposition of heat in the lower corona. It is important to remark that connection of MHD models such as the one presented here to actual heating and acceleration of particles in coronal holes and the solar wind must be done through kinetic theory. A path toward this goal has been conducted during the last years (Leamon et al. 2000; Cranmer 2000). Nevertheless, the model presented here can provide an energy transfer mechanism, in this case turbu-

lence, which can be plugged as a heating source into more fundamental kinetic models.

The s -dependent results of the present model are shown in Figure 6, after time-averaging a solution corresponding to a case with $\eta_{\text{eff}} = 0.6$, $\Delta V_A/V_{\text{AMAX}} = \frac{3}{4}$, and $f = 0.1$. Fluctuation energies (Fig. 6a), of both upward and downward type, are more intense in the first one-third of solar radius height. Downward fluctuations are negligible in the upper part of the domain. Consistently, the normalized cross helicity (Fig. 6c) is almost -1 in the upper region but increases toward the bottom zone. The nonnegligible amount of counterpropagating waves at the bottom region is enough to achieve a sustained level of dissipation there (Fig. 6b). Also shown is the mean square values of fluctuations (Fig. 6d), which differ from the energy in the absence of the weighting factor $\rho \sim 1/V_A^2$. The mean square value is a better way of measuring the level of two-dimensional turbulent fluctuations at each plane. The ratio of downward to upward fluctuations is clearly increasing toward the bottom region, which is also consistent with the level of cross helicity present there. The main result of the s -dependent plots presented here is that dissipation and therefore heating is mainly concentrated in the lower regions of the domain of size R_\odot . A high priority is to pursue the quantitative connection between the present approach and the “dissipation length” formalism that enters solar wind heating theory.

4. CONCLUSIONS

We have applied a model based on the theory of transport of small-scale MHD turbulence (Zhou & Matthaeus

1990) to the problem of heating in open field line regions of the low corona. A reduced MHD description is considered, in which fluctuations are essentially perpendicular to the mean magnetic field. The mean flow is neglected in this low coronal region, compared to the Alfvén velocity. The approach focus on the dynamics of the small-scale fluctuations as influenced by specified large-scale inhomogeneities as well as by local nonlinear couplings. The model incorporates propagation and reflection of Alfvén fluctuations injected at the coronal base, and open boundary conditions are employed. A phenomenological approach (Matthaeus et al. 1999a) is considered for the nonlinear terms, which nonetheless provides insight into the understanding of the interaction among propagation, reflection, and nonlinear effects, and their spatial dependence. The interaction between upward Alfvén waves and their downward reflections provides a driving to a quasi-two-dimensional MHD turbulence, which consists of a nonlinear cascade of fluctuations toward short transverse wavelengths, where efficient dissipation is possible to achieve (for instance, through ion cyclotron damping, although the exact dissipation mechanism is not essential to the present model). Reflections due to gradients of the Alfvén velocity are essential for the model, and we identified the increase of the Alfvén velocity profile over the maximum Alfvén velocity, $\Delta V_A/V_{\text{AMAX}}$ as a relevant parameter. Turbulent heating efficiency increases with this parameter, and we obtained efficiencies of about 30%–40% for reasonable values of coronal parameters. We also studied the asymptotic limit of strong turbulence (which corresponds to small values of the correlation length

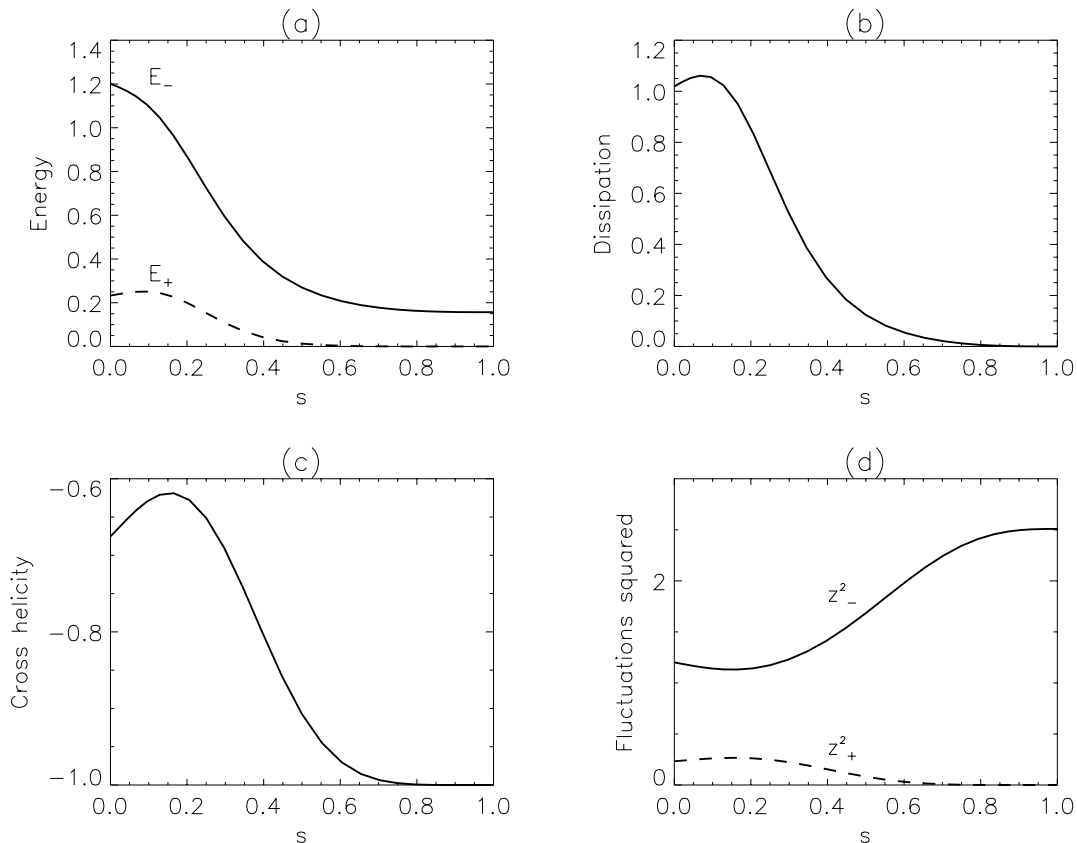


FIG. 6.—Profiles of quantities in the propagation direction s : (a) Energy (includes density factor, proportional to $1/V_A^2$); (b) Dissipation; (c) Normalized cross helicity; (d) Fluctuations squared. For this solution, $\eta_{\text{eff}} = 0.6$, $\Delta V_A/V_{\text{AMAX}} = \frac{3}{4}$, and $f = 0.1$.

that can be identified with the inter-network length at the coronal base) in which case an analytical expression for the heating efficiency can be obtained. Higher efficiencies, approaching exactly the value $\Delta V_A/V_{A,MAX}$, are obtained in this limit. We analyzed the behavior of the model for different values of the frequency of monochromatic wave forcing at the base. Results show that quasi-static (very low frequency) models provide high heating efficiencies and a monotonic downward trend is observed as the forcing frequency increase. It is worth stressing that the low-frequency waves are actually the driver of the system, but reflections and nonlinearities provide a way to cascade energy to small wavelength transverse (i.e., nonpropagating) fluctuations. The mechanism presented for the heating of the coronal plasma so far avoids the possible disadvantages of heating models that rely upon a flux of injected high-frequency waves (Axford & McKenzie 1997; McKenzie et al. 1995; Tu & Marsch 1997), to which there is lacking direct observational evidence.

We also studied the dependence on the coordinate along the propagation direction, and the results indicate that most of the dissipation occurs in the lower region of the domain of one solar radius size considered. In this regard, the present model provides a framework in which the dissipation mechanism, identified as that due to cascade and turbulence, plays the required role of deposition of heat in the lower corona for models of acceleration of the solar wind (McKenzie et al. 1995; Habbal et al. 1995; Evje & Leer 1998) in which a dissipation length in an ad hoc heat deposition term is generally considered. The quantitative connection between our model and the “dissipation length” formalism of solar wind heating and acceleration theories warrants further study.

This work is supported by NASA grants NAG5-7164, NAG5-8134 (SEC Theory Program), and NSF grant ATM 97-13595 to the Bartol Research Institute. We thank Dermott Mullan and Gary Zank for useful discussions.

REFERENCES

- An, C.-H., Musielak, Z. E., Moore, R. L., & Suess, S. T. 1989, *ApJ*, 345, 597
 An, C.-H., Suess, S. T., Moore, R. L., & Musielak, Z. E. 1990, *ApJ*, 345, 597
 Axford, W. I., & McKenzie, J. F. 1997, in *Cosmic Winds and the Heliosphere*, ed. J. R. Jokipii, C. P. Sonnett, & M. S. Giampapa (Tucson: Univ. of Arizona Press), 31
 Coleman, P. J. 1968, *ApJ*, 153, 371
 Cranmer, S. R. 2000, *ApJ*, 532, 1197
 Cranmer, S. R., Field, G. B., & Kohl, J. L. 1999, *ApJ*, 518, 937
 Dmitruk, P., & Gómez, D. O. 1999, *ApJ*, 527, L63
 Dmitruk, P., Gómez, D. O., & DeLuca, E. E. 1998, *ApJ*, 505, 974
 Dmitruk, P., Matthaeus, W. H., Milano, L. J., & Oughton, S. 2001, *Phys. Plasmas*, in press
 Dobrowolny, M., Mangeney, A., & Veltri, P. 1980, *Phys. Rev. Lett.*, 45, 144
 Einaudi, G., Velli, M., Politano, H., & Pouquet, A. 1996, *ApJ*, 457, L113
 Evje, H. O., & Leer, E. 1998, *A&A*, 329, 735
 Gómez, D. O., & Ferro-Fontán, C. 1992, *ApJ*, 394, 662
 Grappin, R., Frisch, U., Léorat, J., & Pouquet, A. 1982, *A&A*, 105, 6
 Habbal, S. R., Esser, R., Guhathakurta, M., & Fisher, R. R. 1995, *Geophys. Res. Lett.*, 22, 1465
 Heinemann, M., & Olbert, S. 1980, *J. Geophys. Res.*, 85, 1311
 Hendrix, D., & van Hoven, G. 1996, *ApJ*, 467, 887
 Heyvaerts, J., & Priest, E. R. 1992, *ApJ*, 390, 297
 Hollweg, J. V. 1981, *Sol. Phys.*, 70, 25
 ———. 1984, *ApJ*, 277, 392
 ———. 1996, in *Solar Wind Eight*, ed. D. Winterhalter, J. T. Gosling, S. R. Habbal, W. S. Kurth, & M. Neugebauer (New York: AIP), 327
 Holzer, T. E., & Axford, W. I. 1970, *ARA&A*, 8, 31
 Hossain, M., Gray, P. C., Pontius, D. H., Jr., Matthaeus, W. H., & Oughton, S. 1995, *Phys. Fluids*, 7, 2886
 Kinney, R., & McWilliams, J. C. 1998, *Phys. Rev. E*, 57, 7111
 Kudoh, T., & Shibata, K. 1999, *ApJ*, 514, 493
 Leamon, R. L., Matthaeus, W. H., Smith, C. W., Zank, G. P., Mullan, D. J., & Oughton, S. 2000, *ApJ*, 537, 1054
 Longcope, D. W., & Sudan, R. N. 1994, *ApJ*, 437, 491
 Mandrini, C. H., Démoulin, P., & Klimchuk, J. A. 2000, *ApJ*, 530, 999
 Marsch, E., & Tu, C. Y. 1993, *J. Geophys. Res.*, 98, 1257
 Matthaeus, W. H., Ghosh, S., Oughton, S., & Roberts, D. A. 1996a, *J. Geophys. Res.*, 101, 7619
 Matthaeus, W. H., Oughton, S., Ghosh, S., & Hossain, M. 1998, *Phys. Rev. Lett.*, 81, 2056
 Matthaeus, W. H., Zank, G. P., & Oughton, S. 1996b, *J. Plasma Phys.*, 56, 659
 Matthaeus, W. H., Zank, G. P., Oughton, S., Mullan, D. J., & Dmitruk, P. 1999a, *ApJ*, 523, L93
 Matthaeus, W. H., Zank, G. P., Smith, C. W., & Oughton, S. 1999b, *Phys. Rev. Lett.*, 82, 3444
 McKenzie, J., Banaszekiewicz, M., & Axford, W. I. 1995, *A&A*, 303, L45
 Montgomery, D. C. 1982, *Phys. Scr.*, T2/1, 83
 Moore, R. L., Musielak, Z. E., Suess, S. T., & An, C.-H. 1991, *ApJ*, 378, 347
 Musielak, Z. E., Fontenia, J. M., & Moore, R. L. 1992, *Phys. Fluids B*, 4, 13
 Oughton, S., Ghosh, S., & Matthaeus, W. H. 1998, *Phys. Plasmas*, 5, 4235
 Oughton, S., Matthaeus, W. H., Dmitruk, P., Milano, L. J., Zank, G. P., & Mullan, D. J. 2001, *ApJ*, in press
 Oughton, S., Priest, E. R., & Matthaeus, W. H. 1994, *J. Fluid Mech.*, 280, 95
 Parker, E. N. 1991, *ApJ*, 372, 719
 Strauss, H. R. 1976, *Phys. Fluids*, 19, 134
 Tu, C. Y., & Marsch, E. 1989, *J. Plasma Phys.*, 41, 479
 ———. 1997, *Sol. Phys.*, 171, 363
 van Ballegooijen, A. A. 1986, *ApJ*, 311, 1001
 Velli, M. 1993, *A&A*, 270, 304
 von Kármán, T., & Howarth, L. 1938, *Proc. R. Soc. London A*, 164, 192
 Withbroe, G., & Noyes, R. W. 1977, *ARA&A*, 15, 363
 Zank, G. P., & Matthaeus, W. H. 1992, *J. Plasma Phys.*, 48, 85
 Zhou, Y., & Matthaeus, W. H. 1990, *J. Geophys. Res.*, 95, 10291